Astron. Astrophys. 321, 927–934 (1997)

ASTRONOMY AND ASTROPHYSICS

The second solar spectrum. A new window for diagnostics of the Sun

J.O. Stenflo[1] **and C.U. Keller**[2]

[1] Institute of Astronomy, ETH Zentrum, CH-8092 Zürich, Switzerland
[2] National Solar Observatory, P.O. Box 26732, Tucson, AZ 85726-6732, USA

Received 2 September 1996 / Accepted 21 October 1996

Abstract. The Sun's radiation becomes linearly polarized by coherent scattering processes in the solar atmosphere. With a novel polarimetry system that achieves a precision of 10^{-5} in the degree of polarization, the previously largely unexplored territory of scattering physics on the Sun is now fully accessible. The observations reveal a polarized spectrum that looks very different as compared with the ordinary, unpolarized solar spectrum but has an astounding wealth of spectral structures. It is therefore refered to as the "second solar spectrum".

In the present paper we show how the second solar spectrum is governed by different physical processes, which provide new diagnostic opportunities and tools that are complementary to those of the ordinary intensity spectrum. We illustrate the effects of quantum interferences and hyperfine structure, isotope abundances, partial frequency redistribution, molecular contributions, and magnetic canopies. Also shown are polarization features, for which the underlying physics has not yet been identified.

Key words: polarization – scattering – Sun: general – techniques: polarimetric – atomic processes

1. Introduction

Molecular Rayleigh scattering is the source of polarization of the blue sky. Similarly, scattering processes on the Sun are sources of polarization in the solar spectrum, even in the absence of external magnetic fields. Thus the continuous spectrum near the Sun's limb is weakly polarized by Thomson scattering at free electrons and Rayleigh scattering at neutral hydrogen. Of greater interest is however the wealth of scattering and coherence effects that can occur between the various discrete states of atoms and molecules. These effects make the polarized spectrum structured with an information content that is very different from that of the ordinary, unpolarized spectrum, since the underlying physical processes are different, as the theory for the scattering physics involved shows (Stenflo 1994, 1996).

Send offprint requests to: J.O. Stenflo

Earlier attempts to explore this domain of physics (Stenflo et al. 1980, 1983a,b) in the solar disk spectrum have revealed a number of unexpected signatures of coherence effects, including quantum-mechanical interference between widely separated atomic states of different total angular momentum (Stenflo 1980). Since however the polarization amplitudes for most spectral lines are on the order of 10^{-3} or smaller, close to the noise level of the instruments previously used, most of the spectrum has remained inaccessible until more sensitive polarimeters could be developed. Such a polarimetric system is now available with ZIMPOL, the **Z**urich **Im**aging Stokes **Pol**arimeter, which by creating more than one image plane within a single Charge Coupled Device (CCD) sensor and shifting the accumulated electric charges rapidly between the image planes in synchrony with the piezoelastic polarization modulation at 42 and 84 kHz rates can entirely eliminate the two main noise sources, which are due to atmospheric seeing fluctuations and inaccuracies in the pixel gain table of the CCD (Povel et al. 1991; Keller et al. 1992; Stenflo et al. 1992; Stenflo 1994; Povel 1995). As the noise is only limited by photon statistics we can routinely achieve a polarimetric accuracy of 10^{-5} when ZIMPOL is being used in combination with the world's largest aperture solar telescope, the McMath-Pierce facility of the National Solar Observatory (Kitt Peak, USA).

At this level of precision the whole solar spectrum is polarized with a structural richness that far exceeded all our expectations (Stenflo and Keller 1996). Due to its different appearance, it is as if the Sun presents us with a completely new spectrum, a treasure that has been hidden from view until now. It is therefore natural to refer to this new spectrum as "the second solar spectrum", a terminology suggested to us by V.V. Ivanov of St. Petersburg (Russia). The task we have before us now is to identify the structures we see and their underlying physics. Once this basic physics is understood we can later proceed to exploit the new spectrum for various applications, e.g. for diagnostics of the Sun's magnetized atmosphere, for radiative transfer physics, or for atomic physics.

The polarization arises because the incident radiation, being anisotropic, induces a net dipole moment in the scattering parti-

cle. If the particle does not suffer a collision before it reradiates, the phase relations between the vector components of the dipole moment (or, in alternate terminology, the coherences between the magnetic substates of the excited state) are preserved and become imprinted on the scattered radiation. An external magnetic field modifies these coherences due to the relative Zeeman shifts of the magnetic substates (corresponding to a precession of the dipole moment). This so-called *Hanle effect* can be very useful for diagnostics of solar magnetic fields in parameter domains where the ordinary Zeeman effect (without coherence phenomena) is insensitive, for instance in prominences (Leroy et al. 1977; Sahal-Bréchot et al. 1977; Bommier 1980; Landi Degl'Innocenti 1982; Querfeld et al. 1985) or for turbulent magnetic fields (Stenflo 1982; Faurobert-Scholl 1993; Faurobert-Scholl et al. 1995). However, to fully exploit the Hanle effect we first need to understand the physical processes responsible for non-magnetic scattering polarization on the Sun.

Local inhomogeneities on the Sun will produce scattering polarization all over the solar disk, but to begin our exploration of this physical domain that is not very familiar to astrophysics, we choose to examine these phenomena for the simplest possible system, namely that of a spherically symmetric sun. For this idealized case the radiative anisotropy needed to give net polarization effects is expressed by the variation of the brightness of the solar disk from center to limb. For reasons of symmetry and scattering geometry the polarization is zero at disk center and increases towards the solar limb, and the plane of linear polarization is oriented either parallel or perpendicular to the nearest limb. If the four Stokes parameters I, Q, U, and V (cf. Stenflo 1994) are defined such that Q represents linear polarization oriented parallel to the nearest limb, then for a spherically symmetric, non-magnetic sun U and V are intrinsically zero, and the degree of linear polarization is Q/I.

To explore this polarization we place the slit of the solar spectrograph close to and parallel to the solar limb at the position angle of geographical north or south, where the influence of solar magnetic fields is small, and integrate for a long time (typically 10 min) to collect enough photons. Instrumental polarization is generally a severe problem in polarimetric observations, since the world's largest solar telescopes have oblique reflections before the point in the optical train where the polarization analysis can be performed. Since in our case, however, the intrinsic Stokes U and V may be assumed to be zero (for the case of a spherically symmetric sun), we only have to be concerned about cross talk from Stokes I (the unpolarized spectrum) into Stokes Q. Cross talk from Stokes Q into I, V, and U may reduce the absolute Q amplitudes somewhat (by less than 0.5 % according to modelling of the telescope), but since the relative amplitudes are not affected and the reduction of the absolute amplitudes is minute, this type of cross talk is not of concern here. When forming the fractional polarization Q/I (which represents the "second solar spectrum"), the Stokes I in the $I \rightarrow Q$ cross-talk term divides out, so that this term becomes spectrally flat. It represents a zero-line offset in the observed degree of polarization, but it cannot produce spurious spectral features. The absolute position of the polarization zero line is therefore unknown in the present observations, so we have to use educated guesses in combination with theoretical predictions of the amount of continuum polarization to choose the zero point in the illustrations that follow.

The assumption that there are no spurious features arising from cross-talk from magnetic-field generated Stokes V (circular polarization) can be checked by looking for spatial variations along the spectrograph slit. Solar magnetic fields are highly structured, while the scattering polarization of a spherically symmetric sun is only a function of center-to-limb distance. In addition, the characteristic anti-symmetric Stokes V profiles produced by magnetic fields are very different from the spectral signatures of the scattering polarization. For a few Fe I lines we found that there was indeed significant Stokes V cross-talk, which was immediately recognized, since its spatial and spectral signatures are so conspicuous. However, in the vast majority of other cases we could verify that no such spurious effects were present (see also below about the high degree of reproducibility of the results).

Let us now present some examples of the second solar spectrum and discuss the underlying physics. All recordings that will be presented have been made with ZIMPOL in April 1995 at the McMath-Pierce facility of the National Solar Observatory (Kitt Peak) with the spectrograph slit positioned 5 seconds of arc inside the north polar limb (where the cosine μ of the heliocentric angle is 0.1).

2. Circular and linear polarization signatures

Figure 1 provides an example of the qualitatively different appearance of the Stokes I, Q/I, and V/I spectra. While V/I shows the spatially fluctuating, anti-symmetric Zeeman-effect profiles for the strongest spectral lines, the Q/I signal often shows up at places where one would not expect it, as in this case for the very weak line of multiplet No. 75 of ionized neodynium, and it is constant along the slit. The strong lines have no positive signal but rather tend to depolarize the background continuum.

The reason why neodynium would be preferred in the scattering polarization is unknown, like the case of numerous other surprises that the "second solar spectrum" has presented us with, some of which will be shown in the present paper. This is not the only Nd II line that shows conspicuous polarization. In any case, we see that $V \rightarrow Q$ cross talk is not dangerous for work near the quiet solar limb, since the Stokes V spectrum has entirely different spectral signatures so that $V \rightarrow Q$ cross talk would immediately be recognized if it occurs in any significant amount.

The spatial variations of V/I along the spectrograph slit shows that the line-of-sight component of the magnetic field reverses its sign approximately every 15 arcsec or has a period of about 30 arcsec, which is the characteristic scale of the Sun's supergranulation. If the fields were vertical we would not expect to see such pronounced line-of-sight components so close to the solar limb. The likely interpretation of what we see is that near the solar limb the line of sight samples a higher layer of

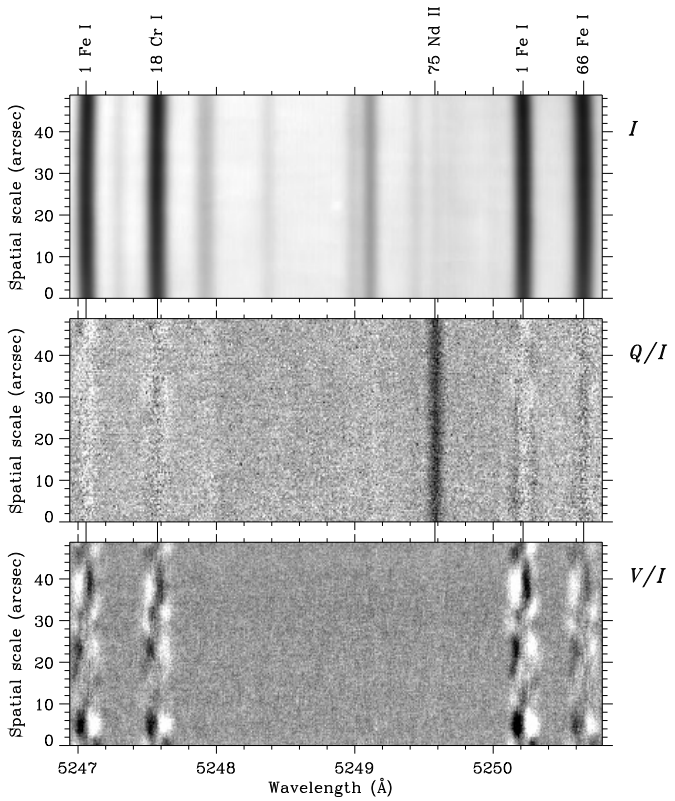

Fig. 1. Examples of the different characters of the ordinary intensity spectrum (Stokes I, top diagram), the linearly polarized spectrum (Stokes Q/I, here called the "second solar spectrum"), and the circularly polarized spectrum (Stokes V/I, bottom diagram). While the circular polarization shows Zeeman-effect signatures due to magnetic canopies at the supergranulation size scale, the linear polarization is dominated by the signature of coherent scattering, which here unexpectedly is due to a transition in ionized neodynium. The recording was made with ZIMPOL at NSO/Kitt Peak with the spectrograph slit parallel to and 5 arcsec inside the north polar limb of the Sun.

the atmosphere than near disk center, and the field of the strong, kG magnetic flux tubes that are largely vertical in the lower photosphere, flare out and becomes almost horizontal in the higher layers due to the exponential pressure drop with height. While the "roots" of the flux tubes are located at the boundaries of the supergranulation cells, the flared out, horizontal fields form "canopies" (Giovanelli 1980; Jones and Giovanelli 1983; Solanki and Steiner 1990) that spread across the supergranular cell until they encounter the flux spreading from other parts of the cell boundary. These horizontal fields would then be expected to fluctuate with the characteristic supergranular scale when observed near the limb with a line of sight that is almost in the horizontal plane and lies up in the canopy region. While the magnetic field is highly bundled and intermittent below the canopy, with a magnetic "filling factor" on the order of 1% , the filling factor approaches unity in the canopy region.

While the polarization amplitude in V/I is a measure of the line-of-sight magnetic *flux*, it does not tell us what the intrinsic field strength is due to the unknown magnetic filling factor when the field is intermittent. To circumvent this problem and diagnose the intrinsic field strength for intermittent, spatially unresolved magnetic fields, the line-ratio technique was invented (Stenflo 1973, 1994) that makes use of the differential effects or polarization ratios between suitably chosen combinations of lines of different Zeeman sensitivities but otherwise identical or at least similar line formation properties. The by far most used such line combination was the 1 Fe I 5247.06/5250.22 Å line pair, which is covered by the spectral range of Fig. 1. For the strong, kG flux tubes in the lower solar atmosphere near disk center the V/I amplitudes of these two lines are approximately the same, while Fig. 1 shows significantly more polarization in the 5250 Å line as compared with the 5247 Å line. For disk-center observations this would have been direct evidence for intrinsically weak fields, but for limb observations the interpretation is not straightforward and requires numerical model calculations before reliable quantitative statements can be made. This is also true for the "thermal" ratio between the amplitudes of the 5250.22 and 5250.65 Å lines, which carries information on the temperature in the magnetic canopy region. The needed numerical modelling is however outside the scope of the present paper.

3. Quantum-mechanical interference, hyperfine structure, and isotope effects

Figure 2 shows some of the most strongly polarizing lines in the visible solar spectrum, the Na I D_2 5889.97 Å and D_1 5895.94 Å lines to the left, the Ba II 4554.04 Å line to the right. The "second solar spectrum" (Q/I) is given in units of % linear polarization (positive means that the electric vector is oriented parallel to the limb, while negative represents the orthogonal direction). The "first solar spectrum" (Stokes I) is given in the upper diagrams, normalized to the intensity I_c of the local continuous spectrum.

Due to their strong polarization signals these lines could be observed in the previous surveys (Stenflo et al. 1980, 1983a,b), but it is only with the sensitivity of the ZIMPOL system that we are able to see with confidence the detailed structure of their polarized line profiles, for instance the narrow polarization peaks in the cores of the D_1 and D_2 lines, and the partially resolved components in the wings of the Ba II line. While the Ba II components in the blue and red line wings can be identified as the hyperfine structure components of the odd Ba isotopes, as shown below (Fig. 3), the overall polarization curve of the Na I D_2–D_1 system is governed by quantum-mechanical interference between the upper $J = \frac{3}{2}$ and $\frac{1}{2}$ states of the D_2 and D_1 lines, respectively. This is the same type of interference effect that could be seen for the Ca II K and H lines at 3933 and 3965 Å and which has been theoretically modeled (Stenflo 1980). A detailed account of the underlying theory can be found in Stenflo (1994).

The polarizability of a scattering transition is determined by the total electronic angular momentum quantum numbers for the levels involved. For atomic transitions without hyperfine structure it is the J quantum number, for cases with hyperfine structure it is the F quantum number that matters. The polarizability is usually expressed in terms of the W_2 factor (Sten-

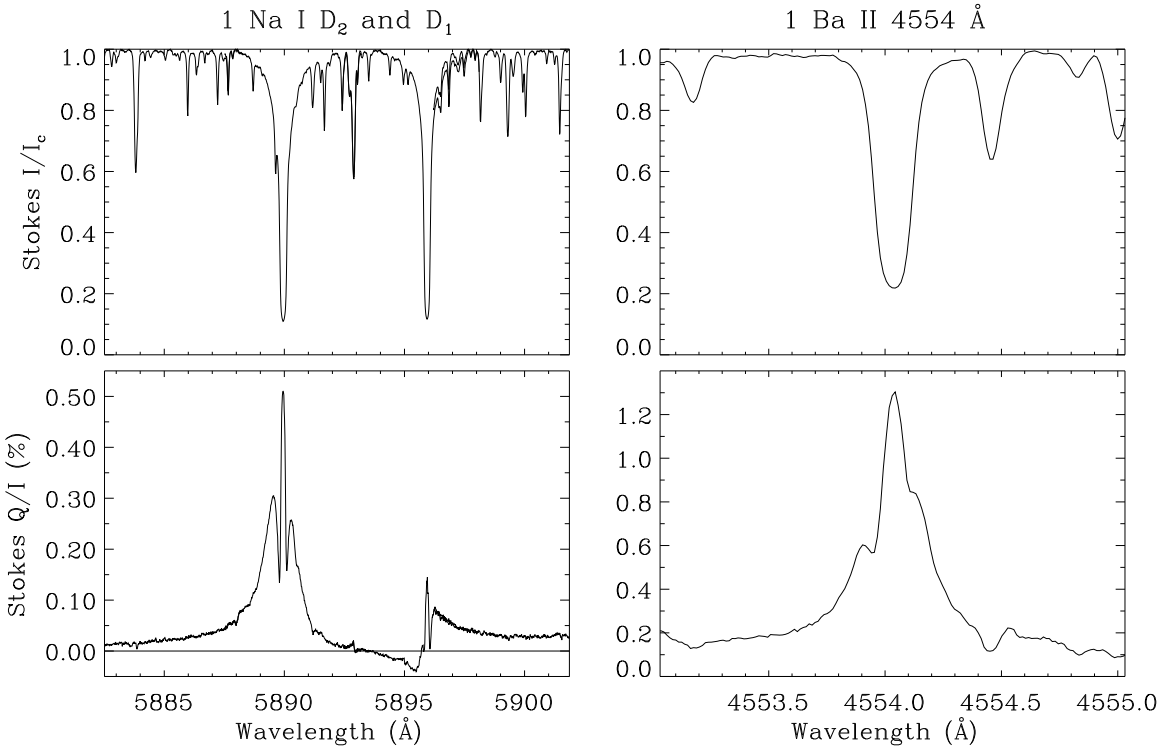

Fig. 2. Examples of signatures of different physical processes that determine the "second solar spectrum" (given as Stokes Q/I, i.e., the degree of linear polarization). While the shape of the polarization curve across the D_2 and D_1 lines of sodium is mainly governed by quantum-mechanical interference between the two upper atomic states with quantum numbers $J = \frac{3}{2}$ and $\frac{1}{2}$, the polarization components in the wings of the Ba II line are due to hyperfine structure splitting in the odd isotopes. The central polarization peak of Ba II is due to the even isotopes.

flo 1994), which represents the fraction of scattering processes that occur as classical dipole scattering. The remaining fraction, $1 - W_2$, corresponds to isotropic, unpolarized scattering. When in a scattering transition more than one upper level is present in the excited state, separated for instance by fine-structure or hyperfine structure splitting, one needs to account for the interference or coherence in the superposition of the contributions from these levels. For a system like Na I D_1 and D_2 with two fine structure components the situation is analogous to the double-slit experiment, when each photon has to pass both slits at the same time. Thus each Na I scattering transition has to go via both excited states at the same time. It is the interference between the states that gives the characteristic and at first sight rather weird polarization signature across the two lines that we see in the bottom left panel of Fig. 2. This interference leads to a frequency dependence of the polarizability factor W_2, in contrast to the case of isolated lines.

In the panel to the upper left of Fig. 3 we have calculated, using our previous theory (Stenflo 1980), the factor W_2 as a function of wavelength for the Na I D_1–D_2 quantum-mechanical system for the case that hyperfine structure is disregarded. The solid line represents the full solution, while the dashed line is the result if we omit the interference term between the two fine-structure components. The solid curve goes asymptotically towards unity when we move away from the resonant wavelengths, which is expected since when the fine-structure splitting becomes unimportant the system becomes independent of the electron spin. In the absence of electron spin, scattering for an $S \rightarrow P \rightarrow S$ transition behaves like classical dipole scattering. This asymptotic behavior is an expression of the principle of spectroscopic stability, which is only obeyed if all the relevant interference terms are taken into account.

If there were no other opacity sources on the Sun than the scattering transition considered, then we would expect the spectral shape of the linear polarization to be approximately proportional to the W_2 that has been determined from pure quantum mechanics, except that the polarization *scale* will depend on the degree of anisotropy of the radiation field in the solar atmosphere. Since however the line transition photons are diluted by continuum photons, we have to give W_2 a wavelength-dependent weight that represents the ratio between the line opacity and the total opacity. This gives us an "effective" W_2, which can be parametrized as follows (Stenflo 1980, 1996):

$$W_{2,\,\mathrm{eff}} = W_2 \, \frac{\varphi_\nu}{\varphi_\nu + a} + b \, \frac{a}{\varphi_\nu + a} \, . \qquad (1)$$

φ_ν represents the area-normalized line opacity profile, which may have superposed contributions from the various transitions that are possible within the considered atomic multiplet, while a is a constant parameter that represents the relative magnitude of the continuum opacity, and b is the constant, effective value of W_2 for the continuum.

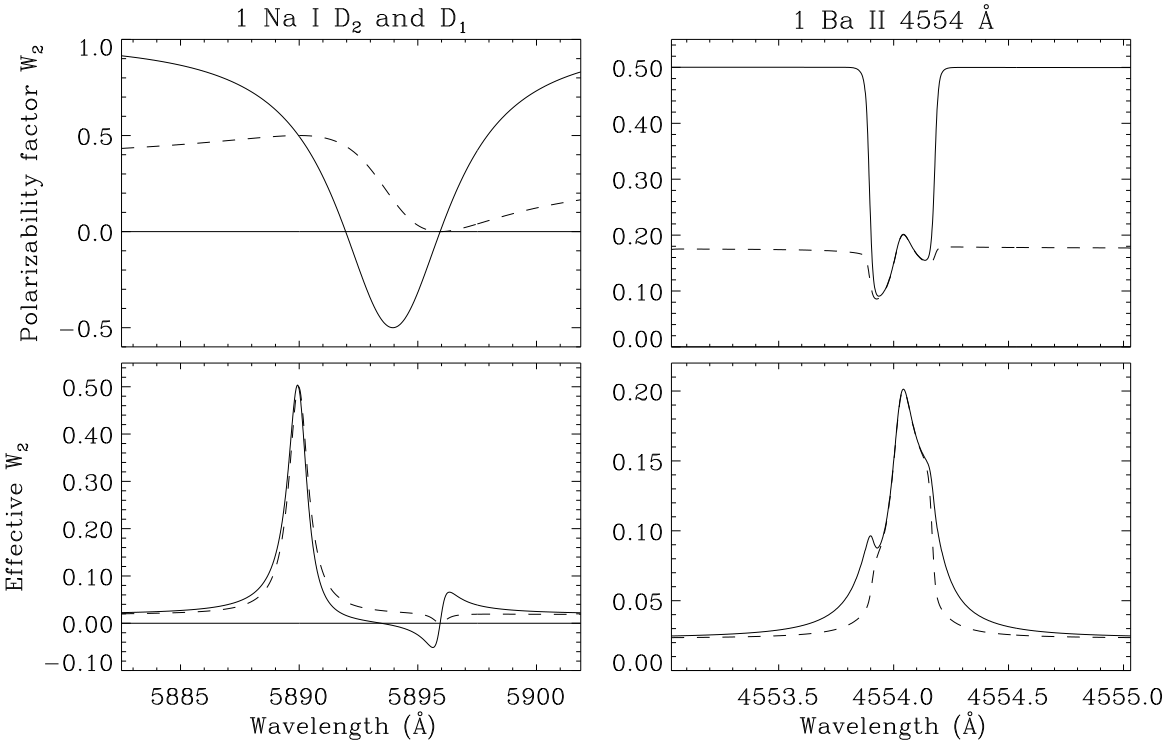

Fig. 3. Quantum-mechanical model calculations to explain the main features of the observed polarization curves in Fig. 2. The upper diagrams give the polarizability factor W_2 as a function of wavelength, while the lower diagrams show how this polarizability is changed into an "effective" W_2 factor when a background continuum that is slightly polarized is added. This simple model provides a surprisingly good representation of the shapes of the observed profiles, apart from the undefined scale factor that is determined by the degree of anisotropy of the radiation field in the solar atmosphere. The solid curves represent the full solution with quantum interferences, while the dashed curves show what happens when the interference terms are omitted.

With a proper choice of the two parameters a and b in the idealized model given by Eq. (1) we obtain from the W_2 diagram to the upper left of Fig. 3 the $W_{2,\,\mathrm{eff}}$ diagram to the lower left. We have here used the values $a = 24.5$ and $b = 0.018$, where a for convenience is expressed in units of the value that φ_ν has at the frequency position halfways between the two resonant frequencies. Apart from the difference in scale, which depends on the degree of anisotropy of the incident radiation field, the theoretical solid curve provides a good representation of the observed gross features of the Na I D_1–D_2 diagram of Fig. 2. The dashed curve shows that when the interference between the $J = \frac{3}{2}$ and $\frac{1}{2}$ states is removed, the S-shaped reversal with negative polarization near the D_1 line does not occur.

The Ba II 4554 Å line transition has the same quantum numbers as the Na I D_2 line, but its corresponding "D_1 line", Ba II 4934 Å, is so far separated from it that quantum-mechanical interference between the two fine-structure components can be neglected. Instead the Ba II 4554 Å line is dominated by effects of hyperfine structure splitting, due to coupling between the electronic angular momentum and the nuclear spin. The Ba II line has contributions from a number of different isotopes, but it is only the odd isotopes that exhibit non-zero hyperfine structure splitting. Calculating the polarizability factor W_2 from the F quantum numbers of the various contributing transitions within the hyperfine structure multiplet while superposing the contributions from the various isotopes in proportion to their relative abundances (using hyperfine structure data for Ba from Rutten (1976)), we obtain the W_2 given in the panel to the upper right of Fig. 3. To simulate the observations we have applied Gaussian broadening to account for Doppler motions on the Sun and instrumental smearing due to the finite spectral resolution. Using with an appropriate choice of the parameters a and b, we obtain the diagram to the lower right, which provides a good representation of the main features of the observed polarization curve in Fig. 2. The parameter values used are $a = 0.000456$ and $b = 0.023$, where in this case (since there are more than two contributing line components) we have chosen to express a in units of the value that φ_ν has at the central frequency of the even isotopes, where the opacity has its maximum (which explains why the numerical value of a is so small).

The polarized components in the blue and red wings of the Ba II line are due to the odd isotopes and their hyperfine structure components, while the central polarization peak is due to the even isotopes. Although the hyperfine structure splitting of the upper level of the atomic transition is very small in comparison with that of the lower level, it has a decisive influence on the polarization profile. Without this small but finite splitting and the interference between the hyperfine structure levels it is

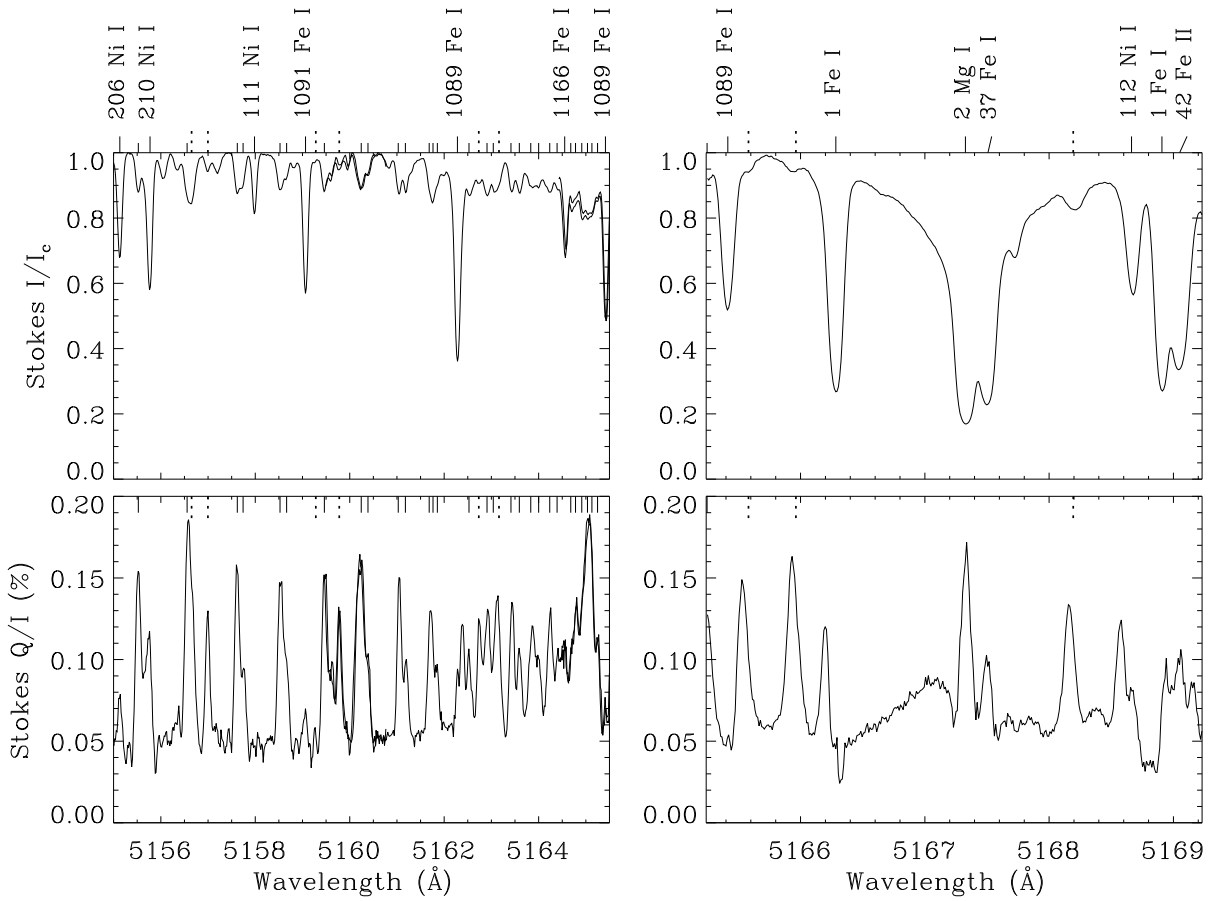

Fig. 4. Examples of molecular features in the second solar spectrum. The wavelengths of identified lines of the C_2 molecule are marked by solid, unlabeled tick marks, those of MgH by dashed tick marks at the top of both the upper and lower panels. A band head of the C_2 Swan system occurs at 5165.2 Å near the right edge of the left panels.

not possible to obtain a good qualitative representation of the observed profile.

Sodium also has nuclear spin and hyperfine structure, although smaller than for Ba. We have calculated the effect of the Na hyperfine structure on W_2 with the aim of modelling the narrow polarization peaks observed in the cores of the D_2 and D_1 lines (cf. Fig. 2) but have found that no choice of model parameters can provide reasonable representations of these peaks. This indicates that the physics behind these features is of different nature. For the peak in the core of the D_2 line we conjecture that partial redistribution effects in polarized radiative transfer could be responsible for at least part of the effect, since a qualitatively similar polarization profile with discrete maxima in the core and wings has previously been found in the Ca I 4227 Å and Ca II K 3933 Å lines (Stenflo et al. 1980, 1983a,b), which have no hyperfine structure, and with the application of partial redistribution it has been possible to explain this feature (Rees and Saliba 1982; Saliba 1985; Frisch 1996).

For the core of the D_1 line, however, we believe that no redistribution effects in radiative transfer will be able to explain the sharp polarization peak, since the intrinsic polarizability W_2 in the neighborhood of the D_1 resonance is close to zero, even when effects of hyperfine structure are taken into account. The reality of this peak is supported by the observation that the corresponding transition at 4934 Å in Ba II also shows a strong and narrow core polarization peak, as illustrated by Fig. 5 below. We will discuss the physical origin of these peaks at the end of Sect. 4.

4. Molecular contributions and unexplained structures

One highly unexpected and surprising feature of the second solar spectrum is the prominence of molecular contributions. Stenflo and Keller (1996) have shown an example of molecular C_2 lines, which are conspicuous in the second solar spectrum while being almost invisible in the ordinary intensity spectrum. Another example is illustrated in Fig. 4. The left panels show a portion of the spectrum with a high concentration of molecular lines. We have marked at the top of both the Q/I and I/I_c diagrams all the wavelengths where the revised Rowland tables of solar wavelengths (Moore et al. 1966) have a listing of a molecular line: The solid, unlabeled "tick marks" indicate the locations of lines of the C_2 molecule, while the dashed tick marks re-

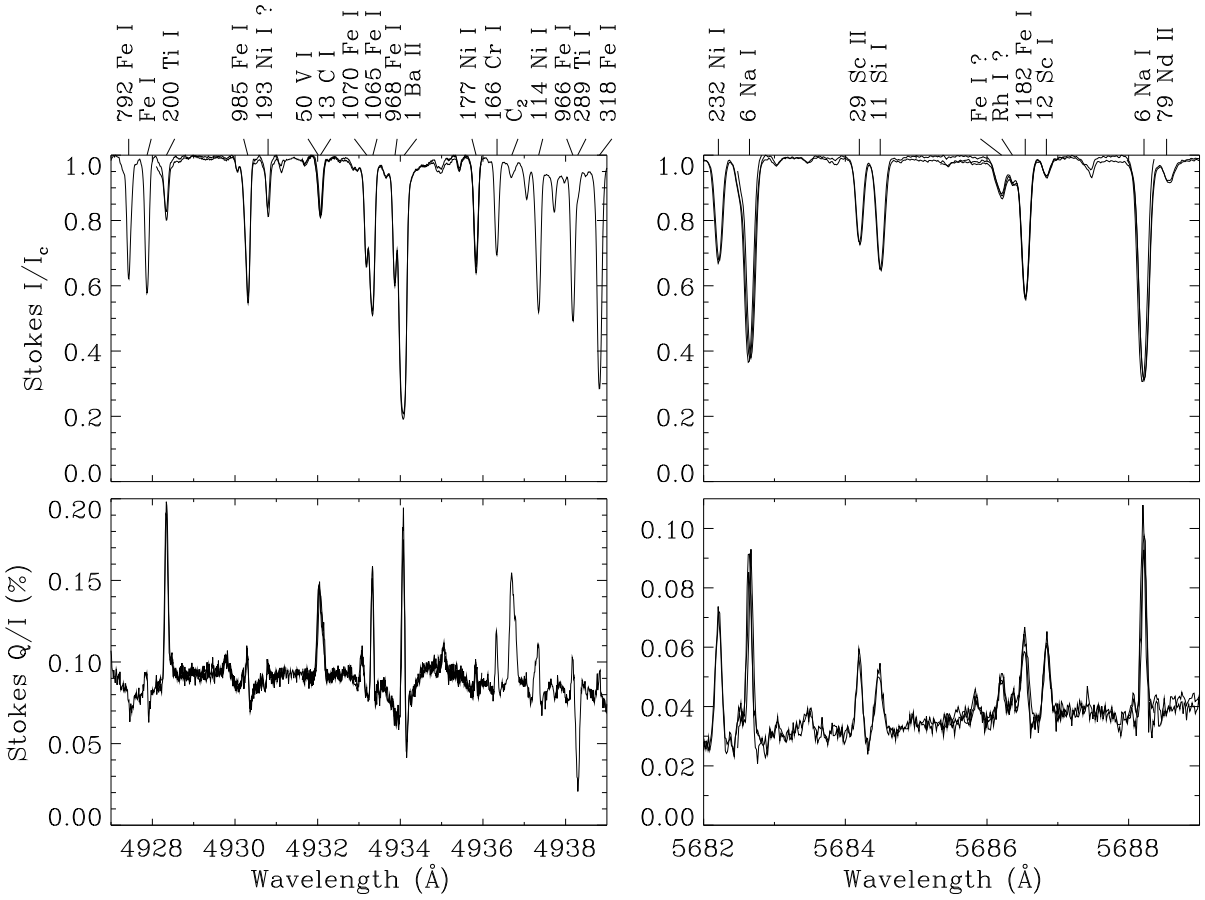

Fig. 5. Examples of the rich structuring and many unexpected atomic contributions to the second solar spectrum. Superposition of recordings made on different days shows that even the smallest polarization features are reproduced.

fer to MgH lines. In addition we have marked and labeled the wavelengths of the other major lines.

The wavelength range shown in the left panels has been covered by several separate recordings, since the spectral field of view of the detector is not large enough to cover the whole range. The overlapping portions of the recordings can be seen where the spectral curves are double in the middle and right part of the wavelength range. They illustrate the degree of repeatability of the results. We see that the overlapping Q/I curves are practically indistinguishable, and that all the spectral features reproduce. The reproducibility is generally better in Q/I than in the ordinary intensity I, since I is subject to gain-table errors and optical vignetting, whereas such effects have divided out in the fractional polarization images. The Na I D_1–D_2 diagram of Fig. 2 also contains several superposed overlapping sections, but the reproducibility is so good that the Q/I spectrum appears as a single curve. The overlapping recordings of Fig. 5 below were made on different days.

The right panels of Fig. 4 provide a detailed view of the region around the strong Mg I 5167.3 Å line. The Rowland tables list three molecular lines in this regions, all of MgH. As seen by the dashed tick marks they correspond to prominent polarization peaks, although these lines are very inconspicuous in the ordinary intensity spectrum in comparison with the adjacent atomic absorption lines. For some reason that we do not yet understand the Sun favors the molecular lines over the atomic lines in the parts of the second solar spectrum that we have been looking at so far, in contrast to the case of the "first solar spectrum".

We have ruled out the possibility of spurious effects by making recordings at disk center, where the intrinsic polarization should be zero, by recording the same spectral region in different grating orders, and by covering half of the slit with a neutral density filter to search for intensity-level effects. All these tests have verified that the observed spectral features are of solar origin and not produced by subtle instrumental effects.

Figure 5 illustrates how all kinds of chemical elements contribute to the second solar spectrum in highly unpredictable ways. We have been able to show by theoretical calculations that fluorescence within the various atomic multiplets plays a fundamental role in shaping the second solar spectrum. Thus often the dominant contributions come from scattering transitions where the initial and final levels are not the same.

The Ba II 4934 Å line in the left panel of Fig. 5 is the other multiplet companion of the Ba II 4554 Å line that was shown in Fig. 2. Like the Na I D_1 line it represents a $J = \frac{1}{2} \rightarrow \frac{1}{2}$ transition and should with this combination of quantum numbers be in-

trinsically unpolarizable ($W_2 = 0$). Its observed pronounced and extremely narrow polarization peak is one of the new intriguing and as yet unexplained effects that we have encountered when we have begun to lift the veil that has been hiding the treasures of the second solar spectrum. We conjecture that both the Ba II 4934 Å and the Na I D_1 polarization peaks are due to transfer of atomic alignment from the $J = \frac{3}{2}$ to the $J = \frac{1}{2}$ level by inelastic collisions. While flipping the direction of the electron spin, this type of collisions would not destroy the alignment of the orbital angular momentum.

5. Concluding remarks

Our first exploratory phase will be followed by applications, using the second solar spectrum (Stokes Q/I) as a new source of information to learn more about atomic physics, abundances and isotope ratios, radiative transfer physics, solar magnetic fields, and the thermodynamics of the solar atmosphere.

The prominent molecular lines in the second solar spectrum provide us with a new source of information on the temperature and pressure structure of the solar atmosphere. Weak atomic lines that are almost invisible in the intensity spectrum may also stand out as conspicuous features in the second solar spectrum. An example that we have found in ZIMPOL observations of February 1996 is the Li I 6707 Å line. Its observed polarization profile gives us a new tool to determine the lithium abundance in the quiet Sun. Relative isotope abundances can also be determined for certain elements, e.g. for barium, since the model fit to the observed polarization profile of the Ba II 4554 Å line is a sensitive function of the assumed abundance ratio between the odd and even isotopes.

We may explore subtle effects in radiative-transfer physics by modelling the polarized profiles of lines like Na I D_2 or Ca I 4227 Å, which are governed by partial redistribution effects. The explanation of the polarization peaks of the D_1 lines of Na I 5896 Å and Ba II 4934 Å may lead to new insights in atomic physics and collision theory.

Magnetic fields that are too weak or tangled to be accessible for diagnostics with the Zeeman effect may be diagnosed from the coherence effects in the second solar spectrum via the Hanle effect. Making use of the differential Hanle effect in combinations of spectral lines it is possible to avoid dependence on sophisticated radiative-transfer calculations for quantitative Hanle diagnostics.

To more fully exploit the coherence phenomena revealed by the second solar spectrum (Stokes Q/I) for magnetic-field diagnostics we need to record the full Stokes vector, not just Stokes I and Q. In the presence of large-scale magnetic fields the Hanle effect causes a rotation of the plane of polarization, and for intermediate and strong magnetic fields the Hanle and Zeeman effects mix in ways that have yet to be explored, although certain regimes of such mixing have been observed (cf. Stenflo 1982). While Hanle depolarization primarily is a diagnostic of magnetoturbulence, we saw in Fig. 1 how the circular polarization near the limb can be used to diagnose the canopy structure of the magnetic field.

Acknowledgements. We wish to thank Marianne Faurobert-Scholl and Jinx Cooper for clarifying discussions. The National Solar Observatory is one of the National Optical Astronomy Observatories, which are operated by the Association of Universities for Research in Astronomy, Inc. (AURA) under cooperative agreement with the National Science Foundation.

References

Bommier, V., 1980, A&A 87, 109
Faurobert-Scholl, M., 1993, A&A 268, 765
Faurobert-Scholl, M., Feautrier, N., Machefert, F., Petrovay, K., Spielfiedel, A., 1995, A&A 298, 289
Frisch, H., 1996, Solar Phys. 164, 49
Giovanelli, R.G., 1980, Solar Phys. 68, 49
Jones, H.P., Giovanelli, R.G., 1983, Solar Phys. 87, 37
Keller, C.U., Aebersold, F., Egger, U., Povel, H.P., Steiner, P., Stenflo, J.O., 1992, LEST Foundation Technical Report No. 53, Univ. Oslo
Landi Degl'Innocenti, E., 1982, Solar Phys. 79, 291
Leroy, J.-L., Ratier, G., Bommier, V., 1977, A&A 54, 811
Moore, C.E., Minnaert, M.G.J., Houtgast, J., 1966, The Solar Spectrum 2935 Å to 8770 Å, NBS Monograph 61
Povel, H.P., 1995, Optical Engineering 34, 1870
Povel, H.P., Keller, C.U., Stenflo, J.O., 1991. In: November L.J. (ed.) Solar Polarimetry. NSO/SP Summer Workshop Ser. No. 11, Sunspot, NM, p. 102
Querfeld, C.W., Smartt, R.N., Bommier, V., Landi Degl' Innocenti, E., House, L.L., 1985, Solar Phys. 96, 277
Rees, D.E., Saliba, G.J., 1982, A&A 115, 1
Rutten, R.J., 1976, PhD thesis, Univ. Utrecht
Sahal-Bréchot, S., Bommier, V., Leroy, J.-L., 1977, A&A 59, 223
Saliba, G.J., 1985, Solar Phys. 98, 1
Solanki, S.K., Steiner, O., 1990, A&A 234, 519
Stenflo, J.O., 1973, Solar Phys. 32, 41
Stenflo, J.O., 1980, A&A 84, 68
Stenflo, J.O., 1982, Solar Phys. 80, 209
Stenflo, J.O., 1994, Solar Magnetic Fields — Polarized Radiation Diagnostics. Kluwer, Dordrecht
Stenflo, J.O., 1996, Solar Phys. 164,1
Stenflo, J.O., Keller, C.U., 1996, Nature 382, 588
Stenflo, J.O., Baur, T.G., Elmore, D.F., 1980, A&A 84, 60
Stenflo, J.O., Twerenbold, D., Harvey, J.W., 1983a, A&AS 52, 161
Stenflo, J.O., Twerenbold, D., Harvey, J.W., Brault, J.W., 1983b, A&AS 54, 505
Stenflo, J.O., Keller, C.U., Povel, H.P., 1992, LEST Foundation Technical Report No. 54, Univ. Oslo

This article was processed by the author using Springer-Verlag LaTeX A&A style file *L-AA* version 3.